Shock Waves

Original article

Flow in near-critical fluids induced by shock and expansion waves

S. Schlamp, T. Rösgen

ETH Zürich, Institute of Fluid Dynamics, Sonneggstr. 3, 8092 Zürich, Switzerland

Abstract. Unsteady shock and expansion waves are proposed as means to produce flows near the liquid-vapor critical-point without imposing pressure gradients. By choosing appropriate initial conditions and wave speeds, near-critical post-wave conditions can be obtained. The post-shock conditions are shown to be stable with respect to perturbations in the pre-shock conditions. The initial conditions are sufficiently far from the critical-point to allow fast thermal equilibration, permitting the use of larger fluid volumes. Example calculations for the cases of an impulsively accelerated piston, of a shock tube, and of a Ludwieg-like tube are presented yielding flows up to 20 m/s in sulfur hexafluoride (SF_6), where the limit is due to the region of validity of the equation of state. The proposed setup also allows one to study shock wave propagation into near-critical fluids.

1 Introduction

Critical phenomena in fluids have obtained a significant amount of attention focusing mostly on the calculation and measurement of thermodynamic and transport properties near the liquid-vapor critical-point [6, 7]. Applications for fluid mechanics beyond those of thermal convection (for thermal transport measurements and the Piston effect) [9, 11–13, 43, 44], shear flows (for viscosity measurements) [8, 22, 31, 32] have been considered only sporadically [1, 18, 23, 33, 34, 40] despite some interesting opportunities, *e.g.* linking the fields of compressible fluid mechanics, critical phenomena, and two-phase flows.

The nonclassical behavior near the liquid-vapor critical-point is not related to the behavior of so-called BZT (Bethe–Zel'dovich-Thompson) fluids, which have a negative fundamental derivative of gas dynamics everywhere or in parts of the flow [3, 4, 15, 16, 25, 38, 39]. Due to its moderate heat capacities, SF_6 does not have a region with retrograde behavior. The nonlinearity, in fact, goes to plus infinity as one approaches the critical-point from any direction in the gas phase [20].

The correlation length of the density fluctuations, typically in the order of angstroms, diverges at the critical-point [10]. Under earth's gravity, it is limited to approx-imately 2 μm, but reaches significantly larger values in reduced-gravity experiments. The macroscopic correlation length then represents an additional length scale for fluid flows. It can be observed on earth in Brownian motion experiments [23, 24], when the size of the particles becomes comparable with the correlation length. For reduced-g environments, scenarios are possible, where the correlation length is comparable to external length scales. Interactions between the critical fluctuations and the mean flow field are then significant.

The speed of sound has a sharp minimum near the critical-point. This feature theoretically allows one to study compressible flows at low Reynolds numbers. The speed of sound near the critical-point for SF_6 is one order of magnitude smaller than in the experiments of Mortimer et al. in a fluorcarbon (FC–43) liquid [29]. In addition, the viscosity diverges at the critical-point [6], which amplifies the effect on the Reynolds number. The speed of sound and the viscosity, like other transport properties, are also strongly frequency dependent even for low frequencies in the critical region [6,17,19,37]. The influence of the dispersion of the speed of sound on transonic flows is another promising field of study, but has been neglected in the present study.

Several factors complicate fluid flow experiments in near-critical fluids:

Correspondence to: S. Schlamp
(e-mail: schlamp@ifd.mavt.ethz.ch)

Table 1. Critical properties of SF$_6$ [41]

@T_c	318.717 K
@p_c	3.7545 MPa
@ρ_c	742 kg/m^3

- Critical phenomena only become significant when the density and the temperature are close to their respective values at the critical-point. While deviations of the density in the order of 1% are typically acceptable, the temperature has to be controlled to within a few millikelvins.
- The thermal diffusivity vanishes at the critical-point. The time required for a fluid sample to reach thermal equilibrium increases rapidly as one approaches the critical-point [23]. Time constants reach hours and even days for sample sizes of a few millimeters thickness.
- The isothermal compressibility diverges at the critical-point. Small pressure gradients result in large changes of the density. Under the influence of gravity, this results in density deviations in the order of 10% over a vertical distance of 10 mm [5]. Hence, pressure-driven flows have to be ruled out in this regime.
- The lack of suitable diagnostic techniques is a problem. When the correlation length becomes comparable to the wavelength of light, critical opalescence is observed, which limits optical techniques to thin fluid samples. Tseng et al. [40] have used MRI to study the flow of liquid and gaseous Xenon.

To produce fluid flow without pressure gradients in a large volume of fluid (not limited in thickness to a few mm), it is proposed here to use unsteady shock and expansion waves.

Example calculations are presented for sulfur hexafluoride (SF$_6$), for which Wyczalkowska and Sengers have developed a crossover equation of state [42]. It shows the correct asymptotical behavior near the critical-point (critical exponents) and regular behavior far away from it. For practical purposes, SF$_6$ is a popular working fluid for experiments because of the convenient location of its critical-point (Table 1) and because it is widely and inexpensively available in high purities.

2 Flow behind unsteady waves

Two cases are considered: the governing equations are introduced for the generic case of an impulsively accelerated piston. With a slight change in notation, they can be applied to the shock tube problem. There, one can chose initial conditions such that either the fluid behind the shock wave or the fluid behind the expansion wave is near-critical. In all cases, a moving, homogeneous fluid region in produced. The pressure gradients are limited to the finite-thickness waves.

2.1 Impulsively accelerated piston

Consider a piston, which closes off one end of a tube or channel. The piston is at rest for $t < 0$, and is accelerated impulsively to velocity $u = u_p$ at $t = 0$, compressing the fluid ahead of it. A shock wave is formed moving with velocity $u_s > u_p$ into the fluid ahead of the moving piston. No information of the moving piston has reached the fluid ahead of the shock wave and it is hence still at rest and at the original density ρ_1, temperature T_1, pressure p_1, and enthalpy h_1. The fluid in the homogeneous region between the shock and the piston (region 2) is moving with $u_2 = u_p$.

The conservation equations for mass, momentum and energy in a shock-fixed coordinate system for a general fluid are given by

$$\rho_1 u_s = \rho_2(u_s - u_p) \qquad (1)$$

$$p_1 + \rho_1 u_s^2 = p_2 + \rho_2(u_s - u_p)^2 \qquad (2)$$

$$h_1 + \frac{1}{2}u_s^2 = h_2 + \frac{1}{2}(u_s - u_p)^2. \qquad (3)$$

Solving Eq. (1) for u_s, substituting into Eqs. (2) and (3), and simplifying yields

$$p_2 = p_1 + \frac{\rho_1 \rho_2}{\rho_2 - \rho_1}u_p^2 \qquad (4)$$

$$h_2 = h_1 + \frac{1}{2}\frac{\rho_2^2 - \rho_1^2}{(\rho_2 - \rho_1)^2}u_p^2. \qquad (5)$$

Given either a pre-shock state (ρ_1, $T1$) or a post-shock state (ρ_2, T_2) and a piston velocity, Eqs. (4) and (5) can be solved numerically for the post-shock condition or the pre-shock condition, respectively. The thermodynamic and the caloric equations of state provide the relations $p(\rho, T)$ and $h(\rho, T)$, respectively. The density and temperature are hence the only unknowns. The ρ-T combinations satisfying Eqs. (4) and (5) form the Hugoniot curve. In general, there are multiple solutions, but only one which satisfies the second law of thermodynamics.

2.2 Shock tube

A finite acceleration of the piston typically results in large steepening distances. A more practical setup to create shock waves is the shock tube.

A high-pressure (driver) and a low-pressure (driven) section are separated by a diaphragm. When the diaphragm bursts at $t = 0$, a shock wave propagates into the driven section, while an expansion wave travels into the driver section. The boundary between the fluids (contact surface) follows the shock, but at a slower speed, into the driven section. Figure 1 shows these processes in x-t-space.

Shock tubes are usually operated by increasing the pressure in the driver section until the diaphragm ruptures. If one requires, as is the case here, that the diaphragm bursts at a certain pressure difference precisely,
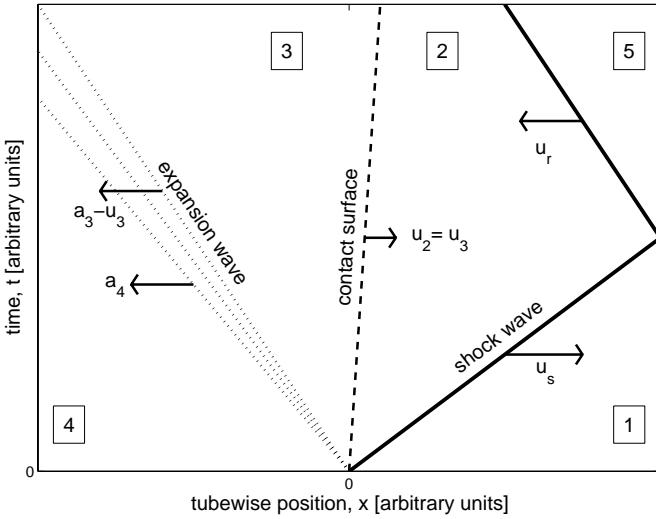
Fig. 1. Wave diagram of shock tube processes. A shock wave travels with speed u_s into the driven section and is reflected at the end wall. The contact surface follows the shock with speed $u_2 = u_3$. The leading and trailing characteristics of the expansion wave travel with speeds a_4 and $a_3 - u_3$, respectively, into the driver section. The reflection of the expansion wave at the driver section end wall is not shown

it can be made to do so either mechanically or by an electrical discharge initiating the rupture process. The same precision can be achieved by using a pair of diaphragms with an intermediate pressure in-between the two initially, and draining the fluid in the gap to initiate the experiment.

The test section or an expansion nozzle are located at the end of the driven section. When the trailing characteristic of the expansion wave moves to the left, (*i.e.*, when $a_3 > |u_3|$), then a test section in the driver section is conceivable. Two subcases have hence to be considered: operating conditions such that the fluid behind the shock wave is near-critical or such that the fluid behind the expansion wave is near-critical.

2.2.1 Critical post-shock conditions

To calculate the required initial states in the driver section (4) and driven section (1) for a desired post-shock flow velocity u_2, one proceeds as follows: First, calculate the Hugoniot as described in Sect. 2.1, replacing u_p by u_2 in Eqs. (4) and (5) and setting $T_2 = T_c$ and $\rho_2 = \rho_c$. This yields the initial conditions in the driven section. The contact surface between regions (2) and (3) cannot support pressure differences. Hence, $p_3 = p_2 = p_c$, *i.e.*, condition (3) lies on the critical isobar. Its exact location is found by the second boundary condition across the contact surface, namely that $u_2 = u_3$. The expansion from (4) to (3) is a left-facing, centered simple wave. u_3 can be found by integrating along the appropriate Riemann invariant [2]

$$J_- = u - \int \frac{dp}{\rho a} = \text{const.,} \qquad (6)$$

which simplifies to

$$\int_0^{u_3} du = -\int_{a_4}^{a_3} \frac{da}{\Gamma(a) - 1} \qquad (7)$$

for homentropic flow. a is the speed of sound and Γ is the fundamental derivative of gas dynamics [38] defined as

$$\Gamma \equiv \frac{v^3}{2a^2} \left(\frac{\partial^2 p}{\partial v^2} \right)_s = 1 + \frac{\rho}{a} \left(\frac{\partial a}{\partial \rho} \right)_s . \qquad (8)$$

One estimates a post-expansion temperature T_3 and iteratively finds the density $\rho_3(T_3, p_3 = p_c)$. One then calculates the isentrope from state (3) up to $T = T_4$, determining Γ along the isentrope using Eq. (8). The speed of sound and entropy are found from the equations of state. u_3 results from integrating Eq. (7). It is then compared with u_2. If $u_3 > u_2$, then T_3 is increased, and vice versa. The correct T_3 is found iteratively by repeating the process until $u_2 = u_3$.

The shock wave is reflected by the end wall of the driven section and propagates back into the now near-critical fluid. The speed of the reflected shock wave, u_r, follows from the conservation equations

$$u_r = \frac{u_2}{\frac{\rho_5}{\rho_2} - 1} \qquad (9)$$

$$p_5 = p_2 + \frac{\rho_5 u_2^2}{\frac{\rho_5}{\rho_2} - 1} \qquad (10)$$

$$h_5 = h_2 + \frac{u_2^2}{2} \frac{\frac{\rho_5}{\rho_2} + 1}{\frac{\rho_5}{\rho_2} - 1} \qquad (11)$$

in terms of the unknowns u_r, T_5, and ρ_5.

In order to obtain near-critical conditions in region (2), the initial state of the driven section has to be in the two-phase region and it is not clear if and how the two-phase fluid can be homogenized sufficiently such that a shock wave propagating through it produces the desired result (see Sect. 4).

2.2.2 Near-critical post-expansion conditions

Because the flow behind the shock wave is subsonic in a fixed frame of reference for the cases considered, the trailing characteristic of the expansion wave is moving to the left (Fig. 1). One can hence also use region (3), the post-expansion wave fluid, as test fluid. This approach is similar to the working principle of the Ludwieg tube [27]. There, one expands into a vacuum, *i.e.* $p_1 = 0$, and steady flow is only achieved in the sense that the *total* temperature and pressure are constant during the test time. Both techniques share the advantage that the level of free-stream turbulence is low, because the fluid is accelerated from rest.

The required initial conditions in the driver and driven sections are calculated as follows: An initial state for the driver section on the critical isentrope is assumed. Starting
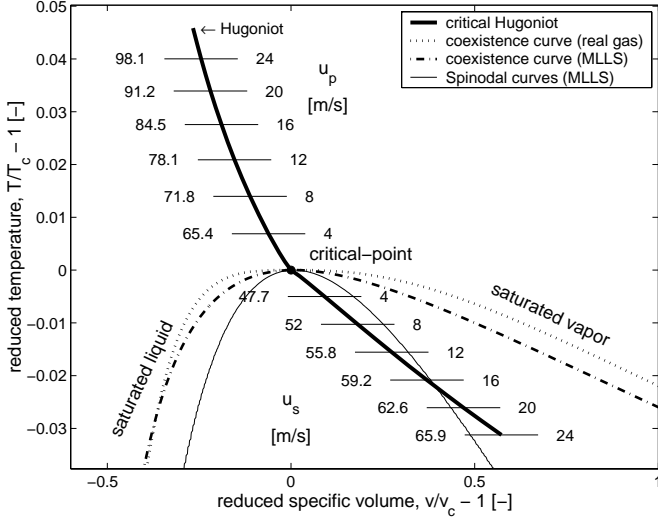
Fig. 2. Both branches of the critical Hugoniot (bold solid line). The upper branch ($T > T_c$) is calculated by setting the pre-shock density and temperature to the critical values and solving Eqs. (4) and (5) for ρ_2 and T_2 given a piston velocity u_p. The lower branch ($T < T_c$) solves for ρ_1 and T_1 assuming $\rho_2 = \rho_c$ and $T_2 = T_c$. The dotted lines are the saturated liquid line and the saturated vapor line. The numerical values to the right and left of the Hugoniot represent the piston velocities and resulting shock speeds, respectively. The dash-dotted and the thin solid lines are the coexistence and spinodal curves, respectively, for the modified Lawal–Lake–Silberberg equation of state

from this guess, Eq. (7) is integrated using Eq. (8) along the critical isentrope up to the critical-point. Iteratively, an improved estimate is found until u_3 has the desired value. Next, a post-shock temperature T_2 is guessed. Because $p_2 = p_3$, this provides an initial estimate for state (2). Solving Eqs. (4) and (5) with $u_2 = u_3$ results in a temperature T_1. By comparing it to the desired temperature a better estimate for T_2 is found, *etc.*

3 Results

3.1 Critical Hugoniot

A subspace trust region method based on the interior-reflective Newton method [14] is used to numerically solve the set of equations consisting of Eqs. (4), (5), and the equation of state for SF_6. The values for the shock speed, u_s, were obtained by substituting the results for the density ρ_1 back into Eq. (1).

Figure 2 shows two Hugoniots: For $T < T_c$, solutions are plotted for critical post-shock conditions and varying values for u_p. For temperatures above T_c, points are plotted, which satisfy the governing equations for critical pre-shock conditions and different piston velocities. The lower branch of the Hugoniot connects conditions, from which the critical-point can be reached by means of a shock wave. The upper branch consists of conditions, which can be reached by a shock wave moving into a near-critical fluid. Like referring to the isobar $p = p_c$ as "critical isobar", the

two branches with critical pre- or post-shock conditions can be referred to as "critical Hugoniot". Note that there can exist other Hugoniot curves, which pass through the critical-point, but for which neither the pre-shock not the post-shock conditions are critical.

Initial states for the lower branch of the critical Hugoniot are in the two-phase region. It is not clear if or how the two-phase mixture can be homogenized sufficiently to treat it as essentially single-phase. The Hugoniot slowly curves upwards while the saturated vapor line curves in the opposite direction. For sufficiently large piston velocities the Hugoniot and the coexistence curve could intersect and so initial states in the gas phase are feasible. Due to a limited range of validity, the location of the intersection point could not be determined with the equation of state used. Even before the intersection with the saturated vapor line, the Hugoniot will cross the spinodal curve. Metastable, single-phase fluids can exist in the area between the spinodal curve and the saturated vapor line (supercooled gas). The equation of state of Wyczalkowska et al. does not provide spinodal curves. Instead, these are shown in Fig. 2 using the modified Lawal–Lake–Silberberg (MLLS) equation of state [26, 36]. This equation yields much better results than the Van-der-Waals or the Peng–Robinson [35] equation near or below the critical point. In particular, the MLLS coexistence curve is much closer to experimental values. Portions of the Hugoniot, however, are always below the spinodal curve and the wave must hence contain two-phase fluid states [21], which could manifest itself in an increased shock thickness.

The entropy change across a weak shock wave for a general fluid is to leading order

$$T_1(s_2 - s_1) = \frac{\Gamma_1}{6} a_1^2 \frac{(v_2 - v_1)^3}{v_1} + \mathcal{O}((\Delta v)^4), \qquad (12)$$

i.e., the entropy increase is only third order in Δv. Points on the Hugoniot close to the critical-point correspond to weak shock waves, and are therefore approximately isentropic. Both branches of the critical Hugoniot are thus tangent to the critical isentrope at the critical-point. For the piston velocities plotted in Fig. 2, the resulting shock waves are weak such that the total entropy increase is small and the critical isentrope would be indistinguishable from the Hugoniot.

Table 2 gives calculated conditions along the upper and lower branches of the critical Hugoniot for a few piston velocities. The jumps in density and pressure are much stronger than the changes in temperature. For the case of $u_p = 8$ m/s, for example, the density changes by 14%, the pressure by 7%, but the temperature by just 1%. This is in partial agreement with weak shock waves in perfect gases, for which one finds

$$\frac{\Delta p}{p_1} \approx \frac{2\gamma}{\gamma + 1}(M_1^2 - 1) \qquad (13)$$

$$\frac{\Delta \rho}{\rho_1} \approx \frac{2}{\gamma + 1}(M_1^2 - 1) \qquad (14)$$

$$\frac{\Delta T}{T_1} \approx \frac{2(\gamma - 1)}{\gamma + 1}(M_1^2 - 1). \qquad (15)$$

Table 2. Conditions along the critical Hugoniot. Left half: $T_2 = T_c$, $\rho_2 = \rho_c$. Right half: $T_1 = T_c$ and $\rho_1 = \rho_c$. The conditions (1) for $u_p = 24$ m/s are outside the region of validity of the equation of state [42] and therefore only approximate

| u_p | lower branch | | | | upper branch | | | |
| | T_1 | ρ_1 | p_1 | u_s | T_2 | ρ_2 | p_2 | u_s |
[m/s]	[K]	[kg/m³]	[MPa]	[m/s]	[K]	[kg/m³]	[MPa]	[m/s]
4	317.122	679.82	3.6247	47.73	320.912	790.30	3.9487	65.44
8	315.444	627.93	3.4931	52.04	323.171	835.05	4.1807	71.79
12	313.756	582.29	3.3649	55.75	325.379	876.77	4.4496	78.07
16	312.074	541.57	3.2413	59.23	327.503	915.19	4.7583	84.55
20	310.407	504.92	3.1224	62.60	329.533	950.32	5.1084	91.24
24	308.759	471.76	3.0084	65.90	331.473	982.45	5.5008	98.06

While the definition of a Mach number near the critical-point or within the two-phase region is not meaningful, we see that the factor in front of the $(M_1^2 - 1)$-term in Eqs. (13)–(15) is smaller for the temperature jump than for the pressure or density jumps. For weak shock waves in perfect gases, however, the pressure jump is larger than the density jump. The opposite is observed here, which is a result of the high compressibility (the isobars are horizontal in the two-phase region). Relative to the variations in u_p, the wave speeds only change slightly (by $\approx 30\%$ for a five-fold increase of u_p). As evident from the kink between the two branches of the critical Hugoniot (Fig. 2), this behavior is slightly less pronounced for the upper branch of the critical Hugoniot.

An important aspect for experiments is the sensitivity of the post-shock conditions to perturbations of the pre-shock conditions or of the piston velocity due to experimental limitations. For perfect gases, the shock jump relations are linear with respect to the pre-shock conditions, *i.e.*, changing the initial density by 1% results in an equivalent change of the post-shock density. This is not true for general fluids. Figure 3 depicts the influence of errors in all three parameters. The post-shock conditions are calculated starting from perturbed pre-shock conditions and for slightly different piston velocities. As starting point, a reference condition is chosen, which requires $u_{p,ref} = 20$ m/s for critical post-shock conditions, corresponding to the entries in the fifth row of Table 2. The perturbations of the initial state are $\pm 0.1\%$ in density, ± 1 mK in temperature and form a rectangle in the T-v-plane. Figure 3 shows the resulting deformed rectangles of the post-shock states in the T-v-plane. The post-shock conditions do neither converge nor diverge near the critical-point. The deviations are approximately twice the perturbations of the initial state. Deviations of the piston velocity by 0.1% result in errors of 5–10 mK.

3.2 Shock tube

3.2.1 Critical post-shock conditions

It is difficult to control the temperatures inside the driver and the driven sections to within mK if $T_1 \neq T_4$. It is
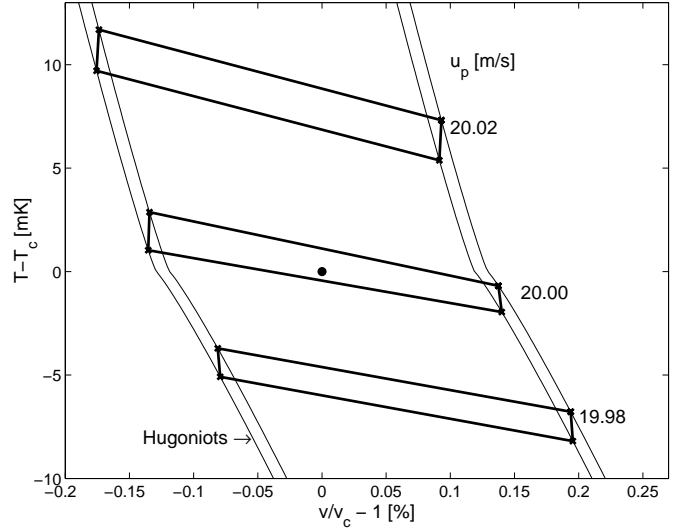

Fig. 3. Sensitivity of post-shock state with respect to perturbations of the pre-shock condition and the piston velocity. Hugoniots are calculated starting from the corners of a rectangle with $\rho_1 = \rho_{1,ref} \pm 0.1\%$ and $T_1 = T_{1,ref} \pm 1$ mK. The deformed rectangles mark the post-shock conditions for $u_p = u_{p,ref} \pm 0.1\%$. The solid circle denotes the critical-point. The kinks in the Hugoniots coincide with the crossing of the saturated liquid/vapor lines

therefore assumed that $T_1 = T_4$. While not required, it is also assumed that SF_6 is used in both sections.

The shock jump relations were calculated as described in Sect. 2.2. The fundamental derivative was determined by second order central finite differencing the speed of sound with respect to the density along 25 equidistant (with respect to temperature) points along the isentrope. An adaptive Lobatto quadrature scheme was used to integrate Eq. (7) where third order cubic interpolation was used for Γ, which changed only gradually (order of 20%) between states (4) and (3) for the cases considered. By construction ($p_4 > p_3 = p_c$ and $T_3 < T_4 = T_1 < T_c$), states (3) and (4) are always in the liquid region of the state diagram.

Figure 4 shows all calculated states for the case of $u_2 = 4$ m/s in a T-v-diagram. Table 3 shows the calculated initial states of the driver and the driven section
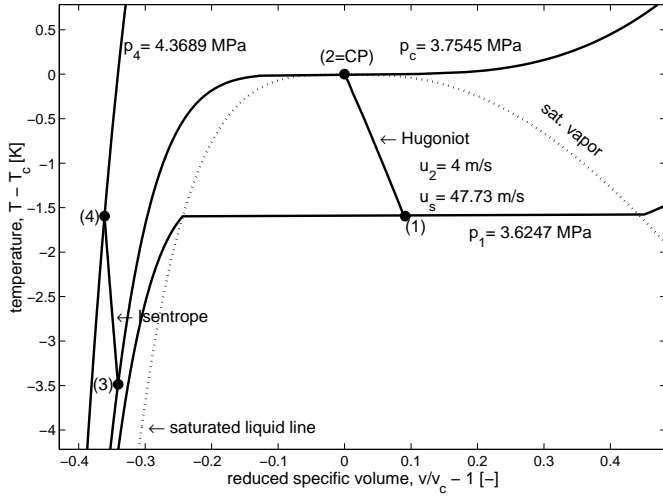
Fig. 4. Shock Hugoniot and expansion in T-v-space for velocity $u_2 = 4$ m/s. The initial state of the driven section is in the two-phase region, while the fluid in the driver section initially is and remains liquid. Metastable initial states (1) exist for higher values for u_2

Fig. 5. Fundamental derivative, Γ, along the critical isentrope

Fig. 6. Speed of sound, a, along the critical isentrope

for different desired flow speeds. The limited region of validity of the equation of state puts an upper bound on the value of u_2, which can be used without sacrificing accuracy. While in Table 2, the lower limit for the temperature $T_1 > 310$ K was responsible, the upper bound of the density $\rho_4 > 1170$ kg/m^3 becomes decisive now.

Note that the left half of Table 3 is identical to Table 2 for $u_2 = u_p$ by construction. The differences in pressure $p_4 - p_1$, which a diaphragm has to support, are in the order of 1 to 2 MPa, and higher for speeds beyond 8 m/s. These values are large if thin diaphragms are to be used, but technically feasible for small cross sections. The performance of a shock tube (measured by shock strength for given pressure ratio $p_4 = p_1$) increases with increasing ratio of sound speeds a_4/a_1. Hence, using N$_2$ or He instead of SF$_6$ in the driver section reduces the required pressure ratio and pressure difference.

3.2.2 Near-critical post-expansion conditions

Because the fundamental derivative diverges as one approaches the critical-point (Fig. 5), the integration of Eq. (7) was stopped 0.1 mK above the critical temperature, which was chosen as T_3. For the same reason, the resolution of the integration was increased. The fundamental derivative was calculated at $1,000$ logarithmically distributed (with respect to $T - T_c$) points along the isentrope. Γ varied by almost four orders of magnitude between states (3) and (4). The behavior of the fundamental derivative and the speed of sound is shown in Figs. 5 and 6, respectively. The fundamental derivative approximately follows a power law near the critical temperature as indicated by the dotted line in Fig. 5, but the curve seems to have a small upward curvature. Similarly, the speed of sound decreases approximately logarithmically for the temperature range shown, but bends slightly up-
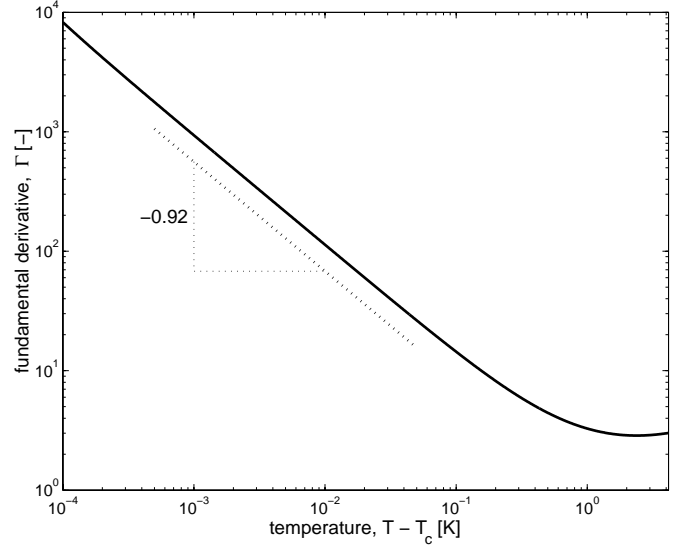
wards (a logarithmic decrease cannot be sustained because the speed of sound cannot become negative).
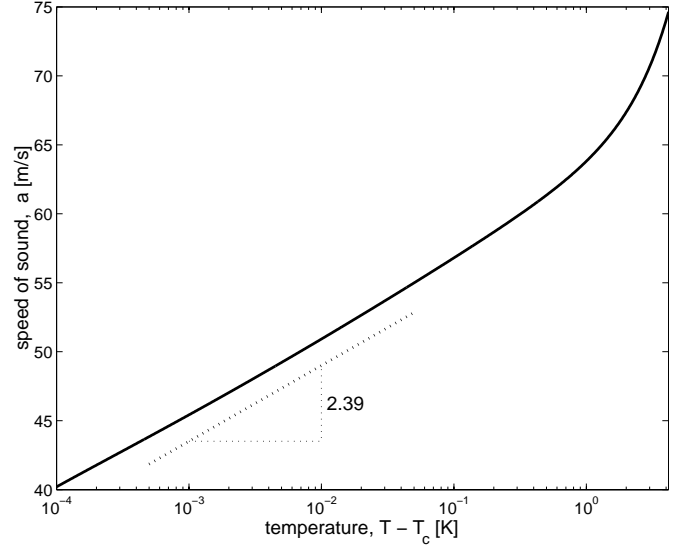
Figure 7 shows the processes in the shock tube, which yield near-critical post-expansion wave conditions. As in Sect. 3.2.1, $T_1 = T_4$ was assumed and the same procedure for the integration along the isentrope was used. All states are single-phase. Table 4 lists operating conditions for a range of flow velocities. a_4 and $a_3 - |u_3|$ are the speeds of the leading and the trailing characteristic of the expansion wave, respectively. Note that $a_3 - |u_3| > 0$ for all cases considered. This means that the trailing characteristic of the expansion wave does indeed move to the left and this scenario is thus possible. The pressure difference $p_4 - p_3$ is between 0.3 and 1.1 MPa, the same order of magnitude as in Sect. 3.2.1.

Table 3. Required initial conditions (1) and (4) in a shock tube to achieve a desired flow velocity u_2 in a near-critical fluid ($T_2 = T_c$, $\rho_2 = \rho_c$). It is assumed that SF$_6$ is used in the driver and the driven section and that $T_1 = T_4$. Note that $u_2 = u_3$ and $p_2 = p_3$. The upper limit for the density of the equation of state of Wyczalkowska and Sengers [42] is 1170 kg/m^3, which is slightly exceeded by the calculated values of ρ_4. The tabulated values are therefore approximate and higher values for u_2 were not calculated

u_2	T_1	ρ_1	p_1	T_4	ρ_4	p_4	u_s	u_r
[m/s]	[K]	[kg/m^3]	[MPa]	[K]	[kg/m^3]	[MPa]	[m/s]	[m/s]
4	317.122	679.82	3.6247	317.122	1161.4	4.3689	47.73	65.04
5	316.705	666.15	3.5916	316.705	1191.0	4.5925	48.91	64.03
6	316.286	652.97	3.5586	316.286	1217.3	4.8360	50.01	63.02
8	315.444	627.93	3.4931	315.444	1263.7	5.3773	52.04	61.05

Table 4. Required initial conditions (1) and (4) in a shock tube to achieve a desired flow velocity u_3 in a near-critical fluid ($T_3 = T_c + 0.1$ mK, $\rho_3 = \rho_c$). It is assumed that SF$_6$ is used in the driver and the driven section and that $T_1 = T_4$. Note that $u_2 = u_3$ and $p_2 = p_3$. The lower limit for the density of the equation of state of Wyczalkowska and Sengers [42] is 336 kg/m^3, which is slightly above the calculated value of ρ_1 for $u_3 = 12$ m/s. These results are therefore approximate and higher values for u_3 were not calculated

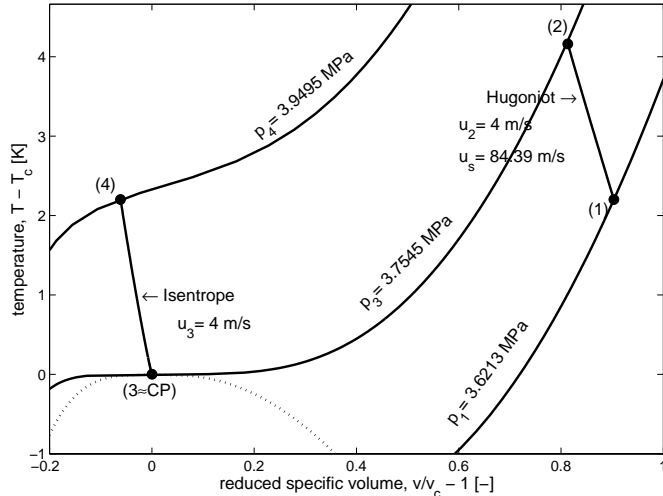| u_3	T_1	ρ_1	p_1	T_4	ρ_4	p_4	a_4	$a_3 - |u_3|$
[m/s]	[K]	[kg/m^3]	[MPa]	[K]	[kg/m^3]	[MPa]	[m/s]	[m/s]
4	320.920	389.84	3.6213	320.920	790.48	3.9495	68.04	36.20
6	322.062	357.23	3.5610	322.062	813.43	4.0621	71.80	34.20
8	323.204	333.32	3.5065	323.204	835.79	4.1845	75.76	32.20
12	325.465	297.45	3.40325	325.465	878.65	4.4615	84.57	28.20

Fig. 7. Shock Hugoniot and expansion in T-v-space for a velocity $u_3 = 4$ m/s. The post-expansion condition (3) is near-critical

4 Summary and conclusions

The concept of the critical Hugoniot was introduced. Its two branches mark all points in state-space, which are either conditions behind a shock wave moving into a near-critical fluid or conditions from which the critical-point can be reached by means of a shock wave.

On the lower branch of the critical Hugoniot, the dependence of the post-shock condition with respect to perturbations of the initial state was shown to be mostly linear. Shock waves do not offer an advantage in terms of the

required accuracy for the density and temperature in the fluid. Instead, an additional parameter (either the piston velocity, or the driver section density and temperature) has to be controlled with similar accuracy. The advantage of the proposed method is that the initial state(s) are away from the critical-point and can thus be reached without encountering the very long equilibration time scales in the vicinity of the critical-point. This allows one to use larger fluid volumes. Secondly, moderate and high flow speeds can be produced without imposing a pressure gradient. The pressure gradient is confined to the shock or expansion wave.

The calculations for the near-critical post-shock conditions only take into account the overall mass, momentum, and energy balance, and do neglect issues arising from the two-phase nature of the pre-shock fluid. It is not clear if and how the two-phase fluid can be homogenized sufficiently. A mechanical mixer, possibly under zero-g, could produce sufficiently small droplets to treat the fluid as essentially single-phase. By using equations of state with a larger region of validity [30], the Hugoniot can be extended towards stronger shocks until the pre-shock state moves into the single-phase region. The two equations of state by Wyczalkowska and Sengers [42] on one hand and of Oda [30] on the other did not show a sufficiently smooth transition of the thermodynamic and caloric properties along the boundary of validity of the former equation of state to switch between them. The former equation, which should be more accurate in the region of interest, was hence used exclusively. In the results presented, the critical Hugoniot does extend into the range of metastable states such that single-phase initial conditions for near-critical

post-shock conditions in a shock tube are possible. Parts of the Hugoniot, however, are always below the spinodal curves. Finite reaction rates for the condensation process thus have to be considered. Also unaccounted for are viscous effects, which could strongly influence the formation and structure of shocks and expansion waves. The issue of two-phase flows is circumvented by considering near-critical post-expansion wave scenarios. Here, all initial and intermediate states are single-phase.

The gravity-induced density profile limits the proximity to the critical-point, which can be achieved with experimental techniques of finite spatial resolution, in isothermal near-critical fluids. Mechanical stirring of a sample can be used to homogenize the density in the sample and to accelerate the equilibration process. This in turn results in an adiabatic gradient, but such a gradient allows one to approach the critical-point more closely than if one had an isothermal profile [10, 28]. The same situation arises in the post-shock region. The advantage of an adiabatic gradient over an isothermal setup becomes even more pronounced in reduced-gravity experiments. The effect of gravity decreases proportionally with g for adiabatic gradients, whereas it decreases as $g^{0.64}$ for isothermal profiles [28].

The proposed setup offers the unique possibility to study the propagation of shock waves in near-critical fluids: The fluid behind the initial shock is near-critical. Hence, if this shock wave reflects from the end wall of the tube, it will propagate back into near-critical fluid.

Depending on the experimental setup, the test time can be limited by the reflected expansion wave reaching the test section, the arrival of the reflected shock wave, or the arrival of the contact surface in the test section. Despite the low wave speeds, typical test times will be in the order of milliseconds due to size constrains, which puts special demands on the diagnostic techniques. For measurements in thin films of near-critical fluids, traditional visualization techniques such as Schlieren or interferometry can be used, but their applicability to larger depths remains to be seen.

References

1. Amiroudine, S., Ouazzani, J., Carles, P., Zappoli, B.: Numerical solution of 1d unsteady near-critical fluid flows using finite volume methods. Eur. J. Mech. B/Fluids **16**(5), 665 (1997)
2. Anderson Jr., J.D.: Modern Compressible Flow With Historical Perspectives. McGraw-Hill, New York, 2nd edition (1990)
3. Argrow, B.M.: Computational analysis of dense gas shock tube flow. Shock Waves **6**(4), 241–248 (1996)
4. Borisov, A.A., Kutateladze, K.C., Nakoryakov, V.E.: Rarefaction shock-wave near the critical liquid vapor point. J. Fluid Mech. **126**, 59–73 (1983)
5. Berg, R.F., Lyell, M.J., McFadden, G.B., Rehm, R.G.: Internal waves in xenon near the critical point. Phys. Fluids **8**(6), 1464–1475 (1996)
6. Berg, R.F., Moldover, M.R., Zimmerli, G.A.: Viscoelasticity of xenon near the critical point. Phys. Rev. Lett. **82**(5), 920–923 (1999)
7. Berg, R.F., Moldover, M.R., Zimmerli, G.A.: Frequency-dependent viscosity of xenon near the critical point. Phys. Rev. E **60**(4), 4079–4098 (1999)
8. Beysens, D., Gbadamassi, M., Boyer, L.: Light-scattering of a critical mixture with shear flow. Phys. Rev. Lett. **43**(17), 1253–1256 (1979)
9. Buschhorn, G., Kilgus, U., Sattler, K.M.: Phase-separating pattern formation in the boundary layer convection of xenon near the gas-liquid critical point. J. Phys.-Condensed Matter **8**(47), 9559–9564 (1996)
10. Cannell, D.S.: Measurement of long-range correlation length of SF6 very near critical-point. Phys. Rev. A **12**(1), 225–231 (1975)
11. Carles, P., Zappoli, B.: The unexpected response of near-critical fluids to low-frequency vibrations. Phys. Fluids **7**(11), 2905–2914 (1995)
12. Carles, P.: The onset of free convection near the liquid-vapor critical point, part II: Unsteady heating. Physica D **147**(1–2), 36–58 (2000)
13. Carles, P., Ugurtas, B.: The onset of free convection near the liquid-vapour critical point, Part I: Stationnary initial state. Physica D **126**(1–2), 69–82 (1999)
14. Coleman, T.F., Li, Y.: On the convergence of reflective Newton methods for large-scale nonlinear minimization subject to bounds. Math. Prog. **67**(2), 189–224 (1994)
15. Cramer, M.S., Kluwick, A.: On the propagation of waves exhibiting both positive and negative nonlinearity. J. Fluid Mech. **142**, 9–37 (1984)
16. Cramer, M.S., Sen, R.: Shock formation in fluids having embedded regions of negative nonlinearity. Phys. Fluids **29**(7), 2181–2191 (1986)
17. Cummins, H.Z., Swinney, H.L.: Dispersion of the velocity of sound in xenon in the critical region. Phys. Rev. Lett. **25**(17), 1165–1169 (1970)
18. Denny, D.L., Pego, R.L.: Models of low-speed flow for near-critical fluids with gravitational and capillary effects. Quart. Appl. Math. **58**(1), 103–125 (2000)
19. Eden, D., Garlan, C.W., Thoen, J.: Sound absorption and dispersion along the critical isochore in xenon. Phys. Rev. Lett. **28**(12), 726–729 (1972)
20. Emanuel, G.: Analysis of a critical point with application to fluid mechanics. AME Report 96-1, School of Aerospace and Mechanical Engineering, University of Oklahoma (1996)
21. Fergason, S.H., Ho, T.L., Argrow, B.M., Emanueal, G.: Theory for producing a single-phase rarefaction shock wave in a shock tube. J. Fluid Mech. **447**, 37–54 (2001)
22. Fuller, N.G., Rowley, R.L.: Nonequilibrium molecular dynamics simulation of shear viscosity of polar liquids. Int. J. Thermophys. **19**(4), 1039–1048 (1998)
23. Gitterman, M.: Hydrodynamics of fluids near a critical point. Rev. Mod. Phys. **50**(1), 85–106 (1978)
24. Gitterman, M.: Brownian motion in fluctuating media. Phys. Rev. E **52**(1), 303–306 (1995)
25. Lambraki, K.C., Thompson, P.A.: Existence of real fluids with a negative fundamental derivative. Phys. Fluids **15**(3), 933 (1972)

26. Lawal, A.S., Van der Laan, E.T., Thambynayagam, R.K.M.: Four-parameter modification of the Lawal-Lake-Silberberg equation of state for calculating gas-condensate phase equilibria. Soc. Pet. Eng. of AIME, Pap. 14269 (1985)

27. Ludwieg, H.: Der Rohrwindkanal. Z. Flugwiss. **3**, 206–216 (1955)

28. Moldover, M.R., Sengers, J.V., Gammon, R.W., Hocken, R.J.: Gravity effects in fluids near the gas-liquid critical point. Rev. Mod. Phys. **51**(1), 79–99 (1979)

29. Mortimer, B.J.P., Skews, B.W., Felthun, L.T.: The use of a slow sound speed fluorocarbon liquid for shock wave research. Shock Waves **8**(2), 63–69 (1998)

30. Oda, A., Uematsu, M., Watanabe, K.: An equation of state for sulfur hexafluoride in the range of temperatures 222 K to 500 K up to 50 MPa. Bull. JSME – Jpn. Soc. Mech. Eng. **26**(219), 1590–1596 (1983)

31. Onuki, A.: Phase transitions of fluids in shear flow. J. Phys. Condensed Matter **9**(29), 6119–6157 (1997)

32. Onuki, A., Yamazaki, K., Kawasaki, K.: Light-scattering by critical fluids under shear-flow. Ann. Phys. **131**(1), 217–242 (1981)

33. Onuki, A., Kawasaki, K.: Critical phenomena of classical fluids under flow. 1. Mean field approximation. Prog. Theor. Phys. **63**(1), 122–139 (1980)

34. Onuki, A., Kawasaki, K.: Critical phenomena in two-dimensional incompressible flows. Suppl. Prog. Theor. Phys. **69**, 146–159 (1980)

35. Peng, D., Robinson, D.B.: New two-constant equation of state. Ind. Eng. Chem. Fund. **15**(1), 59–64 (1976)

36. Super, M.S., Beckman, E.J., Enick, R.M.: Near-critical and supercritical fluid densities of CO2-SF6 mixtures. Fluid Phase Equ. **86**, 275–292 (1993)

37. Thoen, J., Garland, C.W.: Sound absorption and dispersion as a function of density near the critical point of xenon. Phys. Rev. A **10**(4), 1311–1327 (1974)

38. Thompson, P.A.: A fundamental derivative in gas dynamics. Phys. Fluids **14**(9), 1843–1849 (1971)

39. Thompson, P.A., Lambraki, K.C.: Negative shock-waves. J. Fluid Mech. **60**, 187–208 (1973)

40. Tseng, C.H., Mair, R.W., Wong, G.P., Williamson, D., Cory, D.G., Walsworth, R.L.: Magnetic resonance imaging of laser polarized liquid xenon. Phys. Rev. E **59**(2), 1785–1788 (1999)

41. Wagner, W., Kurzeja, N., Pieperbeck.: The thermal behavior of pure fluid substances in the critical region – experiences from recent pT measurements on SF6 with a multi-cell apparatus. Fluid Phase Equ. **79**, 151–174 (1992)

42. Wyczalkowska, A.K., Sengers, J.V.: Thermodynamic properties of sulfurhexafluoride in the critical region. J. Chem. Phys. **111**(4), 1551–1560 (1999)

43. Zappoli, B., Amiroudine, S., Carles, P., Ouazzani, J.: Thermo-acoustic and buoyancy-driven transport in a square side-heated cavity filled with a near-critical fluid. J. Fluid Mech. **316**, 53–72 (1996)

44. Zappoli, B., Amiroudine, S., Gauthier, S.: Rayleigh-Taylor-like instability in near-critical pure fluids. Int. J. Thermophys. **20**(1), 257–265 (1999)